Optimization of transmit parameters for two-dimensional cardiac strain estimation with coherent compounding *in silico, in vitro,* and *in vivo*.

Vincent Sayseng[1], Julien Grondin[1], Clement Papadacci[1], Alexandre Costet[1], Elisa Konofagou[1].
Department of Biomedical Engineering
Columbia University
New York, NY, USA
vincent.sayseng@gmail.com

***Abstract*—Coherent compounding has been investigated as a possible means of increasing strain estimation accuracy while retaining high frame rate; however, the optimal parameters that yield the best strain estimate have yet to be determined. Three transmit parameters were investigated: the number of transmits, the subaperture size, and the angular aperture. Field II simulations of an annular region mimicking cross-sectional views of the systolic left ventricle were imaged. The highest number of transmits evaluated (15), the smallest subaperture (11 elements), and the narrowest angular aperture (60°) were found to yield the smallest axial and lateral interframe strain errors. A hemi-ellipsoid PVA phantom was inflated and deflated in a water tank to generate wall strain, and the *in silico* results were corroborated by the phantom results. Finally, a canine infarct model was employed wherein the LAD was ligated, and open chest images of the myocardium were acquired four days later. *In silico* and *in vivo* results were used to design an optimized compounding sequence featuring 11 transmits, a 21 element subaperture, and a 90° angular aperture. Based on TTC staining of the excised heart, the optimized sequence was able to distinguish between healthy and infarcted tissue, whereas the single diverging wave sequence incorrectly estimated strain in several regions. This optimization study indicates that a higher number of transmits, a small subaperture, and a narrow angular aperture yield the most accurate strain estimate.**

Keywords*—*elastography, cardiovascular disease, ultrasound imaging

I. INTRODUCTION

Myocardial Elastography uses normalized cross-correlation to estimate strain in two-dimensions in an angle-independent fashion; by using RF data to estimate the polar and principal strains as opposed to relying on the B-mode, ME can leverage both phase and intensity to accurately estimate displacement [1]. The success of ME is reliant on a high frame rate; an insufficient frame rate invites estimator decorrelation due to the volatility and velocity at which the heart contracts, inevitably leading to inaccurate strain estimation [2]. Coherent compounding of diverging waves has shown to be capable of producing B-mode images of comparable quality to those generated with focused transmits, while relying on fewer transmissions, thus enabling a higher frame to be achieved [3]–[5]. Recently, coherent compounding has also been shown to improve strain estimation quality[5], [6]. However, the ideal transmit parameters that will maximize strain estimation accuracy are yet unknown.

This paper will aim to determine the optimal transmit parameters for ME myocardial strain imaging with coherent compounding of diverging waves and parallel beamforming. Specifically, three transmit parameters will optimized: number of transmits, subaperture size, and angular aperture. Our group has shown in previous work that based on simulation and in vivo studies of healthy humans, a higher number of transmits leads to better strain estimation [7], [8]. However, to the authors' knowledge, no work has yet investigated the effect of subaperture size and angular aperture on 2D cardiac strain estimation. Transmit number, subaperture size, and angular aperture will be investigated *in silico* via Field II simulations of an annular region mimicking cross-sectional views of the heart, *in vitro* with a PVA hemiellipsoid phantom that replicates the left ventricle, and *in vivo* with a canine infarct model to compare an optimized compounding sequence with a singular diverging wave sequence.

II. METHODS

A. Three transmits parameters in ME with coherent compounding

Coherent compounding with diverging waves was employed to improve RF signal quality, thereby enhancing strain estimation accuracy. Diverging waves are generated by setting virtual sources behind the transducer element array. Three critical transmit parameters are the number of diverging waves transmitted, subaperture size in number of elements, and angular aperture in degrees The number of virtual sources dictates the number of transmits to be coherently compounded, and the distance of the virtual sources from the element array is defined by the subaperture size and angular aperture. Subaperture size is defined as the number of elements activated during transmission. The following constraint was applied in

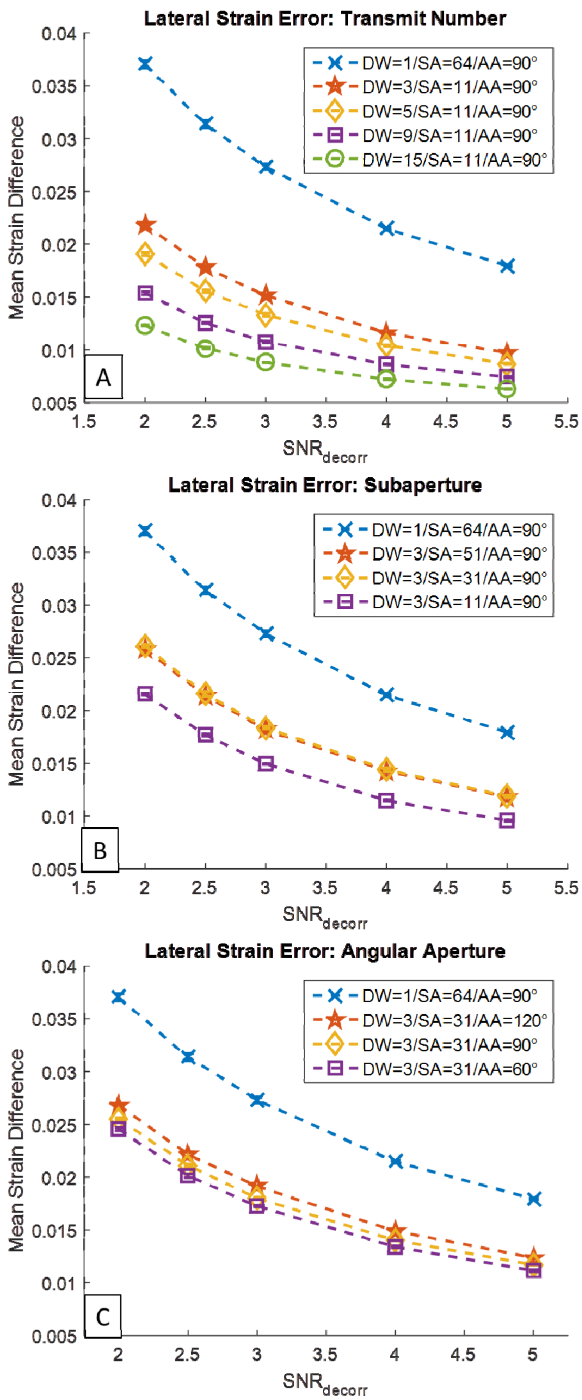

Fig 1. Field II simulation results showing how the three transmit parameters affected interframe lateral strain in an annular region undergoing symmetric radial deformation over 100 frames.

this paper: the transmitted wave must be symmetrical, thus forcing the virtual source to be centered over the subaperture. Transmits were spaced to maximize distance between virtual sources while retaining transmit wave symmetry. All elements were used during receive. Angular aperture Φ_{AA} is defined as the angle created by the vectors from the virtual source to the ends of the subaperture. For brevity, number of diverging waves, subaperture size, and angular aperture may be referred to in shorthand as DW, SA, and AA, respectively. Under this nomenclature, a singular diverging wave sequence employing all elements during transmit with a 90° insonication field-of-view would be described as DW=1/SA=64/AA=90°.

B. *Field II*

The A 2D annulus undergoing symmetric radial thickening was created in Field II to simulate short-axis cross-sectional views of the systolic left ventricle. The annulus had a radial thickness of 20 mm, and underwent a radial interframe displacement of 0.05 mm over 100 frames for a total cumulative radial displacement of 5 mm. Based on analysis of interframe displacement observed during the large animal portion of this study, 0.05 mm displacement roughly equates to a 500 fps frame rate. In order to simulate decorrelation, white noise was filtered to have same power spectrum as the RF data, and then the two signals were summed. The amplitude of the RF signal relative to that of the decorrelation signal, or SNR$_{decorr}$, reflects the level of decorrelation to be simulated. Decorrelation was randomized between transmits. After beamforming, a 1D cross-correlation kernel was applied in a 2D search to determine axial and lateral displacements [9]. Axial and lateral interframe strains were calculated with a least-squares estimator (LSQSE). Strains were converted from polar to Cartesian coordinates before analysis. In order to evaluate strain estimate accuracy, theoretical interframe axial and lateral strains were calculated throughout the entirety of the virtual phantom walls over all 100 frames of systole. Given an axial or lateral interframe 3D strain matrix of n by m by k dimensions (where n and m are spatial coordinates and k is time), error in strain estimation was defined as the mean of the point-by-point absolute difference between the estimated and theoretical strain matrices, normalized by the number of points in each matrix.

The three transmit parameters—number of virtual sources, subaperture size, and angular aperture—were evaluated over a SNR$_{decorr}$ range of 2 to 5. In regards to the number of transmits, the subaperture size and angular aperture were set to 11 elements and 90°, while the number of transmits was varied at 3, 5, 9, and 15 waves. To evaluate subaperture size, the number of transmits and angular aperture were set to 3 sources and 90°, while the subaperture was varied at 11, 31, and 51 elements. To assess the effect of angular aperture, the number of transmits and subaperture size was set to 3 sources and 31 elements, while angular aperture was varied at 60°, 90°, and 120°. The sequence DW=1/SA=64/AA=90° was also evaluated over an SNR$_{decorr}$ range of 2 to 5 to allow comparison between a single transmit sequence and a variety of compounded transmit sequences. Five virtual phantoms were generated and imaged with the aforementioned sequences to account for potential variability in RF data generation by Field II. The mean strain differences were averaged across these 5 simulations.

C. *Phantom Study*

A hemiellipsoidal phantom was created by casting a polyvinyl alcohol (PVA) gel in a 3D-printed ABS plastic mold. The phantom possessed a 10 mm thickness, 60 mm height (apical surface to base), and a 50 mm outer diameter at the base. A large syringe (12 oz/stroke) was connected to a three-

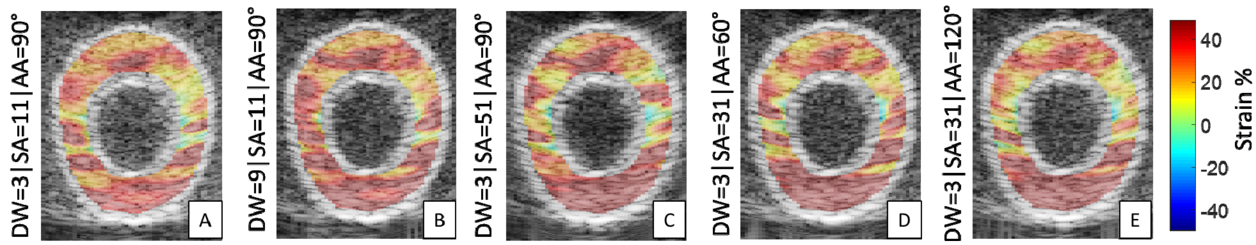

Fig 2. Cumulative radial strain derived from hemiellipsoid phantom experiment. Specific sequence is defined to the left of each strain image

way axis positioner. Tubing connected the syringe to a waterproof box (Pelican 1060 Micro Case, Torrance, CA). A 50 mm hole was made at the center of the case top. The phantom's symmetric radial flange at the base kept the phantom adhered to the box when an adequate internal pressure was achieved. A Verasonics Vantage system (Verasonics, Redmond, WA) and 2.5 MHz ATL P4-2 phased array probe was used to image the phantom. Launching an acquisition triggered the positioner to inject water into the box, causing the phantom to inflate and its walls to undergo negative radial strain. The positioner would then immediately retract, causing the phantom to deflate, with its walls undergoing positive radial strain. This inflate-deflate cycle would complete in 1.3 seconds.

The phantom was imaged with the following sequences at 250 fps : DW=3/SA=11/AA=90° versus DW=9/SA=11/AA=90° to evaluate the impact of increasing the number of transmits; DW=3/SA=11/AA=90° versus DW=3/SA=51/AA=90° to determine the effect of subaperture size; and DW=3/SA=31/AA=60° versus DW=3/SA=31/AA=120° to investigate the influence of angular aperture on strain estimation. Acquisition depth was set to 11 cm. Strain estimation accuracy was evaluated qualitatively by inspection of the cumulative axial, lateral, and radial strains.

D. *Large Animcal infarct study*

An adult mongrel dog (n=1) weighing 25 kg was employed in this study. After placing the canine under anesthesia, a veterinary surgeon performed a lateral thoracotomy to expose the myocardium. The LAD coronary artery was dissected and occluded via a 2-stage ligation, thereby creating an anteroseptal myocardial infarct. The incision was closed and the dog was survived for 4 days, undergoing a postoperative care program incorporating antibiotics and pain management. On the last day, a lateral thorocatomy was performed to expose the heart for open-chest imaging using two sequences, DW=1/SA=64/AA=90° and DW=11/SA=21/AA=90°. After imaging, the dog was euthanized and the heart excised. All method used here were in compliance with the Institutional Animal Care and Use Committee of Columbia University. The myocardium was sectioned into cross-sectional slices, submerged in 1% tetrazolium chloride (TTC) solution for 15 minutes at 37° C, and then submerged in 10% Formalin solution for an additional 5 minutes.

The imaging sequence used in this experiment combined acquisitions for DW=1/SA=64/AA=90° and DW=11/SA=21/AA=90°. One transmit set consisted of 11 diverging waves followed by a singular full aperture diverging wave. The sequence featured a pulse repetition frequency (PRF) of 6000 Hz, leading to a frame rate of 500 fps for both sequences. This sequence design ensured that both sequences would be evaluated in the exact same imaging conditions.

III. Results

A. *Optimization of transmit parameters with Field II*

Strain estimation performance was evaluated by determining the mean strain difference between the estimated and theoretical interframe axial and lateral strains, as summarized in Fig. 1. All transmit configurations show a decrease in mean strain difference as SNR_{decorr} increases, denoting an improvement in strain estimation accuracy. All configurations where the number of transmits are 3 or greater (DW $\geq$ 3) show marked improvement in strain estimation accuracy compared to the singular diverging wave sequence, DW=1/SA=64/AA=90°.

Lateral interframe strain performance *in silico* while varying the number of transmits is summarized in Fig 1A (axial interframe strain results showed similar patterns). Aside from the singular diverging wave sequence, subaperture size and angular aperture were set to 11 elements and 90°. Interframe mean strain difference decreased axially and laterally as the number of transmits was increased from 3 to 15 for all levels of SNR_{decorr}, with DW=15 providing the most accurate strain estimates. Increasing the number of transmits lent the most improvement in low SNR_{decorr} conditions; conversely, when decorrelation was low (i.e. when SNR_{decorr} was high), the improvement in strain estimation error achieved by increasing transmit number was much smaller.

Lateral interframe strain estimation *in silico* is summarized in the middle row of Fig. 1B (axial interframe strain results showed similar patterns). Aside from the singular diverging wave sequence, the number of transmits and angular aperture were set to 3 waves and 90°. A subaperture of 11 elements showed a significant improvement in axial and lateral interframe mean strain difference relative to the larger subapertures. Over the entire range of SNR_{decorr}, a reduction in mean strain difference of approximately 13% and 18% axially and laterally, respectively, was achieved with a subaperture size of 11, compared to 31 and 51 elements.

Fig. 1C summarizes the effect of angular aperture on lateral interframe strain performance *in silico* (axial interframe strain results showed similar patterns). With the exception of the singular diverging wave sequence, the number of transmits and subaperture size was set to 3 waves and 31 elements. As the angular aperture was decreased from 120° to 60°, interframe mean strain difference decreased axially and laterally for all levels of SNR_{decorr}. An angular aperture of 60° decreased interframe strain error by 13% and 8% axially and laterally compared to a larger aperture of 120°.

B. Optimization of transmit parameters with a myocardial PVA phantom

Phantom radial strains corroborated with simulation results. DW=9 (Fig. 2B), SA=11 (Fig. 2A), and AA=60° (Fig. 2D) sequences features more homogenously and uniformly positive radial strains compared to their experimental counterparts, DW=3 (Fig. 2A), SA=51 (Fig. 2C), and AA=120° (Fig. 2E), respectively. That is, a lower number of transmits, smaller subaperture, and narrower angular aperture lead to superior radial cumulative strain results.

C. Optimization of transmit parameters via canine infarct model

TTC staining of the excised canine myocardium revealed that an infarct was successfully created in the anteroseptal region (Fig. 3A). Cumulative radial strain images taken with the compounded sequence (DW=11/SA=21/AA=90°) correctly identified the location of the infarct as an area exhibiting zero or very low positive strain, while healthy areas of the heart show robust positive strains ≥30% (Fig. 3B). In comparison, the singular diverging wave sequence (DW=64/SA=64/AA=90°) incorrectly identified the entire anterior region of the heart as infarcted (Fig. 3C). Furthermore, the positive strains reported in the posterior and lateral regions of the heart are less spatially homogeneous compared to the compounded sequence; the posterior region, in particular, could be identified as an ischemic or infarcted region.

IV. Conclusion

Coherent compounding with parallel beamforming allows high frame rate imaging without compromising spatial resolution. In investigating three critical transmit parameters related to ME with coherent compounding, it has been shown in silico and in vitro that a high transmit number, small subaperture size, and narrow angular aperture return the most accurate strain estimates. All configurations of compounding were found to estimate strain with lower errors compared to a single diverging wave sequence. An optimized compounding sequence employing 11 transmits, a 21 element subaperture, and a 90° angular aperture was successfully used to differentiate between infarcted and normal myocardium in a canine infarct model.

Acknowledgment

Supported in part by NIH funding (EB006042 and HL094410).

References

[1] E. E. Konofagou, J. D'hooge, and J. Ophir, "Myocardial elastography—a feasibility study in vivo," *Ultrasound Med. Biol.*, vol. 28, no. 4, pp. 475–482, Apr. 2002.

[2] E. A. Bunting, J. Provost, and E. E. Konofagou, "Stochastic precision analysis of 2D cardiac strain estimation in vivo," *Phys. Med. Biol.*, vol. 59, no. 22, pp. 6841–6858, Nov. 2014.

[3] B. Holländer, G. A. G. M. Hendriks, R. M. Mann, H. H. G. Hansen, and C. L. de Korte, "Plane-Wave Compounding in Automated Breast Volume Scanning: A Phantom-Based Study," *Ultrasound Med. Biol.*, Jul. 2016.

[4] G. Montaldo, M. Tanter, J. Bercoff, N. Benech, and M. Fink, "Coherent plane-wave compounding for very high frame rate ultrasonography and transient elastography," *IEEE Trans. Ultrason. Ferroelectr. Freq. Control*, vol. 56, no. 3, pp. 489–506, Mar. 2009.

[5] C. Papadacci, M. Pernot, M. Couade, M. Fink, and M. Tanter, "High-contrast ultrafast imaging of the heart," *IEEE Trans. Ultrason. Ferroelectr. Freq. Control*, vol. 61, no. 2, pp. 288–301, Feb. 2014.

[6] H. H. G. Hansen, A. E. C. M. Saris, N. R. Vaka, M. M. Nillesen, and C. L. de Korte, "Ultrafast vascular strain compounding using plane wave transmission," *J. Biomech.*, vol. 47, no. 4, pp. 815–823, Mar. 2014.

[7] J. Grondin and E.E. Konofagou, "Cardiac strain imaging with coherent compounding of diverging waves in sillico." submitted for publication.

[8] E. Bunting, C. Papadacci , J. Grondin, V. Sayseng, and E. E. Konofagou, "Improvements in Two-Dimensional Cardiac Strain Estimation in vivo using Coherent Spatial Compounding", submitted for publication.

[9] W.-N. Lee, C. M. Ingrassia, S. D. Fung-Kee-Fung, K. D. Costa, J. W. Holmes, and E. E. Konofagou, "Theoretical Quality Assessment of Myocardial Elastography with In Vivo Validation," *IEEE Trans. Ultrason. Ferroelectr. Freq. Control*, vol. 54, no. 11, pp. 2233–2245, 2007.

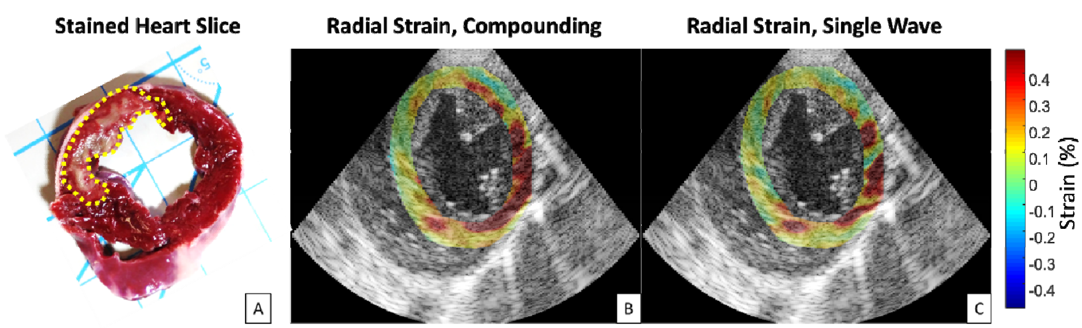

Fig 3**.** Results of canine infarct model experiments. **A**. Cross-section slice of excised canine myocardium after TTC staining. Note the anterior-septal infarct, outlined with a dotted yellow line. **B.** Radial strain observed with an optimized compounded sequence, DW=11/SA=21/AA=90. **C.** Radial strain observed with singular diverging wave sequence, DW=1/SA=64/AA=90.